Letters

An Ultrafast and Wide-Safe-Range Start-Up Method of DAB Converters With Straightforward Frequency-Phase Closed-Loop Control

Linxiao Gong, *Student Member, IEEE*, Yunfeng Peng, Chaofan Cui, Jie Chen, Lingfeng Jiang, Xing Fang, Jian Wang, Junzhong Xu, and Yong Wang, *Member, IEEE*

***Abstract*—Fast and safe start-up is crucial for the dual-active-bridge (DAB) converters. Conventional closed-loop start-up controls fail to achieve theoretical maximum power output due to manually predefined phase-shift modes, limiting start-up speed and safe operational range. To address these issues, this letter proposes a novel variable frequency plus extended phase-shift (EPS) control. This approach enables ultrafast and wide-safe-range start-up of DAB converters by maximizing power-per-current-stress capability within safety limitations. In addition, sole EPS modulation is required in the proposed control, thus eliminating complex mode transitions and streamlining the start-up process. Experimental results indicate that the proposed control achieves a broader safe start-up range and improves start-up speed by up to 43% under voltage-match condition compared to the state-of-the-art methods.**

***Index Terms*—Dual active full bridge, power per current stress (PPS), start-up, variable frequency plus phase-shift control.**

I. Introduction

DUAL-ACTIVE-BRIDGE (DAB) converters are vital in uninterruptible power supply systems, providing backup power support for dc grids, more electric aircraft, and data centers. During emergencies, achieving a safe and fast start-up is essential for rapid access of backup power [1].

During the start-up process, DAB converters rapidly charge the output capacitor and operate under extremely low-voltage gain conditions, leading to high inrush peak current and potential power device failures. Consequently, a series of open-loop start-up methods has been proposed in [2], [3], and [4] to suppress the inrush current. Typically, during the open-loop stage, the secondary side switches are turned OFF, allowing the system to function as a rectifier bridge. Once the voltage reaches the threshold, closed-loop control is implemented to achieve the reference voltage. These methods [2], [3], [4] often require segmented mode transitions and meticulous manual fine-tuning of parameters, thereby limiting their applicability.

Consequently, closed-loop-only start-up methods have garnered significant research interest. In [5], an output-voltage-based dynamic boundary control with single phase-shift (SPS) modulation is proposed to expedite the start-up process. With the development of advanced phase-shift modulation in [6], extended phase-shift (EPS) and triple phase-shift (TPS) control featuring trapezoidal current modulation (TZM) are selected under the buck condition to fasten the start-up process under current stress limitation. In [7], a two-mode EPS control with enhanced output power is employed to further speed up the process. Despite that various advanced phase-shift controls are adopted in [6] and [7], the theoretical maximum output power under given current stress limitations still cannot be fully achieved due to manually predefined phase-shift modes, thus constraining start-up speed and safe operational range (as detailed in Section II).

To address aforementioned issues, a power-per-current-stress (PPS) factor is established to quantify the start-up ability under current stress limitations, and a novel variable frequency plus continuous-current-based EPS control with the highest PPS ability is proposed in this letter. The main contributions are as follows.

1) *Ultrafast start-up speed:* Derived from mathematical analysis, the continuous current modulation (CCM) phase-shift control offers the highest PPS ability compared to controls in [5], [6], and [7], significantly accelerating the start-up process.
2) *Expanded safe start-up range:* Combined with frequency regulation, the maximum PPS capability can be maintained and extended to any current stress requirement, thereby expanding the safe start-up range.
3) *Simplified control:* Only a single CCM pattern (a type of EPS control) is required in the whole start-up process, simplifying the control system.

The rest of this letter is organized as follows. In Section II, the flaws of state-of-the-art start-up controls are discussed in detail. Section III analyzes a phase-shift pattern with maximized PPS

Manuscript received 16 June 2024; revised 21 July 2024; accepted 2 August 2024. Date of publication 6 August 2024; date of current version 11 September 2024. This work was supported by China Postdoctoral Science Foundation under Grant 2022M722057. *(Corresponding author: Yong Wang.)*

Linxiao Gong, Chaofan Cui, Jie Chen, Lingfeng Jiang, Xing Fang, Junzhong Xu, and Yong Wang are with the Key Laboratory of Control of Power Transmission and Conversion of Ministry of Education, Shanghai Jiao Tong University, Shanghai 200240, China, and also with the Department of Electrical Engineering, Shanghai Jiao Tong University, Shanghai 200240, China (e-mail: gonglx@sjtu.edu.cn; 2086473240@sjtu.edu.cn; chenjie1026@sjtu.edu.cn; lingfengjiang@sjtu.edu.cn; xingfang@sjtu.edu.cn; junzhongxu@sjtu.edu.cn; wangyong75@sjtu.edu.cn).

Yunfeng Peng is with the Key Laboratory of System Control and Information Processing of Ministry of Education and the Department of Automation, Shanghai Jiao Tong University, Shanghai 200240, China (e-mail: pengyf@sjtu.edu.cn).

Jian Wang is with the College of Smart Energy, Shanghai Jiao Tong University, Shanghai 200241, China (e-mail: wj1071268395@sjtu.edu.cn).

Color versions of one or more figures in this article are available at https://doi.org/10.1109/TPEL.2024.3439396.

Digital Object Identifier 10.1109/TPEL.2024.3439396

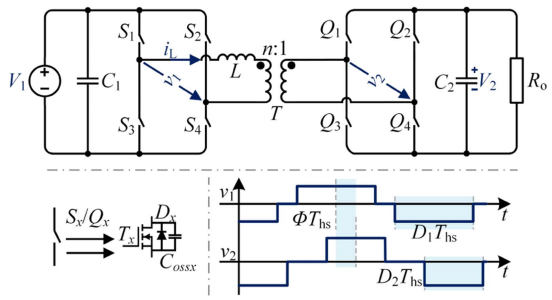

Fig. 1. Topology of DAB converters and the definitions of phase-shift angles. The DAB converter consists of two H-bridges with AC voltages denoted by v_1 and v_2 and transformer T with a leakage inductance L and a turns ratio n:1.

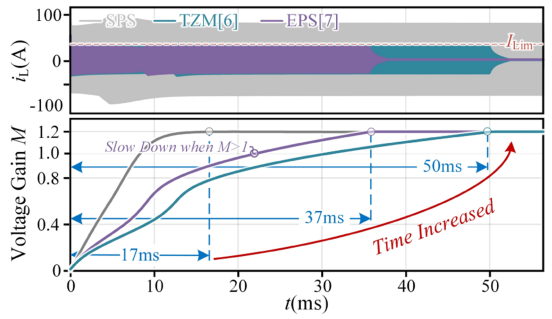

Fig. 2. Prolonged start-up time of TZM and EPS, where $M = 1.2$, $P_o = 0$ W, $I_{\rm Lim} = 30$ A, and other parameters are identical to those in Table II.

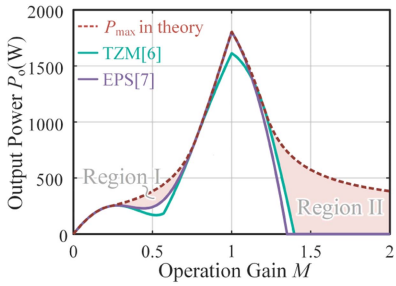

Fig. 3. Maximum output power of TZM and EPS control under $I_{\rm Lim} = 0.35I_N$. I_N represents the maximum stress of DAB and $I_N = V_1/(4f_sL)$.

ability and explores the feasibility of frequency regulation. In Section IV, the variable frequency plus continuous current modulation (VF+CCM) control is developed, and its characteristics are analyzed. Experimental results are presented in Sections V. Finally, Section VI concludes this letter.

II. Flaws of State-of-the-Art Start-Up Controls

The topology of DAB converters and the definitions of phase-shift angles discussed in this letter are illustrated in Fig. 1. The voltage gain M is defined as $M = nV_2/V_1$. For state-of-the-art closed-loop start-up controls [6], [7], flaws can be summarized and detailedly described as follows.

A. Slow Start-Up Speed

The start-up processes in TZM [6] and EPS [7] are illustrated in Fig. 2. To ensure a safe start-up, the current stress of the

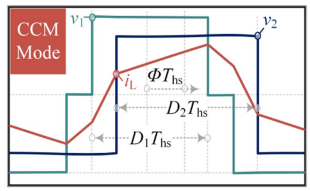

Fig. 4. Control pattern of CCM modes (a type of EPS control).

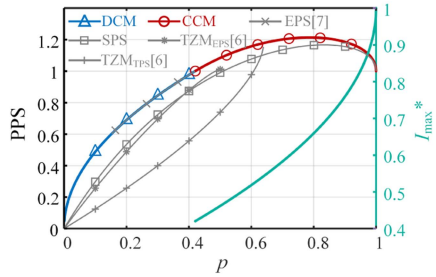

Fig. 5. PPS ability comparison between various controls under $M = 0.7$, where per unit power $p = P_o/P_N$, and per unit current stress $I^*_{\rm max} = I_{\rm max}/I_N$.

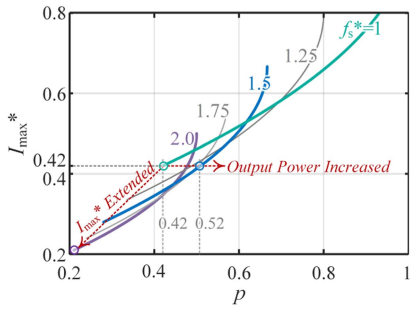

Fig. 6. Current stress variation of CCM control with f^*_s, where $f^*_s = f_s/f_{\rm steady}$, where $f_{\rm steady}$ represents the switching frequency under steady operation.

inductor must be maintained within safety limits to protect the devices. Consequently, the current stress limitation $I_{\rm Lim}$ is proactively considered in the design of phase-shift controls in [6] and [7]. However, since the current stress of DAB converters is positively related to the output power, the inclusion of current limiting would weaken output power ability, thereby extending start-up time to two to three times longer compared to SPS control.

B. Narrow Safe Range

The output power curves under $I_{\rm Lim}$ in TZM and EPS are shown in Fig. 3. $P_{\rm max}$ represents the theoretical maximum power with phase-shift modulation obtained through iterative MATLAB searches. Regions I and II correspond to the theoretical power gap between the two controls and $P_{\rm max}$ under $M < 1$ and $M > 1$. As illustrated, the primary power gap occurs in region II, where both EPS and TZM transition to SPS control, leading to a sharp decrease in P_o under $I_{\rm Lim}$. Furthermore, as M increases, P_o in both the algorithms drops to zero when $M > 1.3$, meaning that safe start-up cannot be achieved under high-voltage gain conditions.

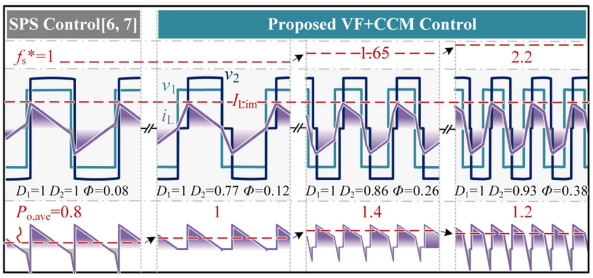

Fig. 7. Analysis of power increasing reason in VF+CCM control under $M = 1.3$.

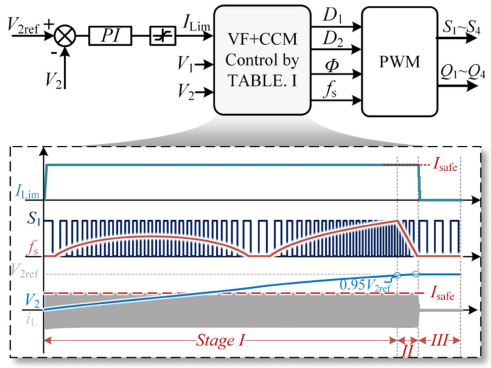

Fig. 8. System closed loop of the proposed VF+CCM control.

Therefore, to enhance the speed and safe range of the start-up process, it is essential to maximize output power under I_{Lim} and maintain this capability across a wide voltage range.

III. Maximum PPS Pattern

First, the following optimization target should be established to maximize output power under I_{Lim}:

$$\begin{cases} I_{\max} = f(D_1, D_2, \Phi) \cdot I_N = I_{\mathrm{Lim}} \\ \max\{P = f(D_1, D_2, \Phi) \cdot P_N\} \end{cases}. \tag{1}$$

By combining the power and current stress expressions of DAB converters under various phase-shift modes [8], optimal control laws can be obtained by Karush–Kuhn–Tucker conditions. For example, under $M < 1$, optimal control would locate in two modes

$$\mathrm{DCM}\left\{D_1 = \frac{I_{\mathrm{lim}}}{2(1-M)}, D_2 = \frac{D_1}{M}, \Phi = \frac{I_{\mathrm{lim}}}{4M}, P_{\max} = \frac{I_{\mathrm{lim}}^2 P_N}{2M(1-M)}\right.$$

$$\mathrm{CCM}\begin{cases} D_1 = 1 - \frac{(1-I_{\mathrm{lim}})(M-1)}{(M-1)^2+M^2}, D_2 = 1 \\ \Phi = 0.5 - \frac{0.5M(1-I_{\mathrm{lim}})}{(M-1)^2+M^2}, P_{\max} = 1 - \frac{(1-I_{\mathrm{lim}})^2 P_N}{(M-1)^2+M^2} \end{cases} \tag{2}$$

where $I_{\mathrm{lim}} = I_{\mathrm{Lim}}/I_N$, $P_N = nV_1V_2/(8f_sL)$, and corresponding applicable I_{lim} range is DCM:$0 \le I_{\mathrm{lim}} \le 2M(1-M)$ and CCM: $2M(1-M) \le I_{\mathrm{lim}} \le 1$. The pattern of CCM mode is illustrated in Fig. 4.

Herein, a PPS factor is defined to quantify the start-up ability under I_{Lim} requirement, calculated as $\mathrm{PPS} = p/I_{\max}^*$. According to (2) and the control laws in [6] and [7], the PPS ability in different controls can be obtained and illustrated in Fig. 5. As

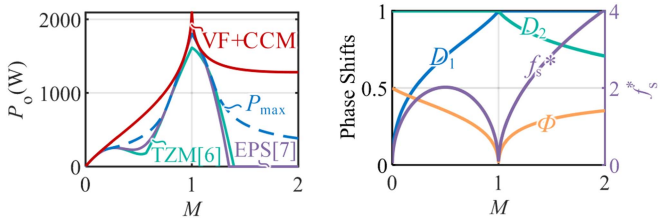

Fig. 9. Key features of different controls. (a) Power comparison under $I_{\mathrm{Lim}} = 0.35I_N$. (b) Control variables of VF+CCM.

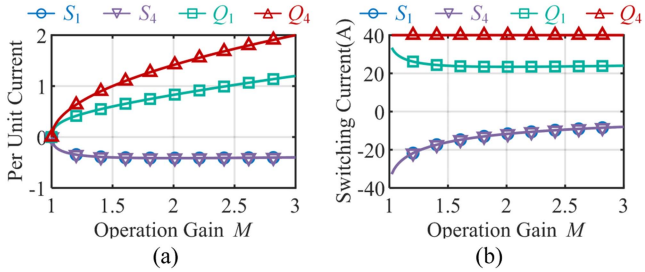

Fig. 10. Switching currents of all the switches under the boost condition. (a) Per unit current. (b) Practical switching current.

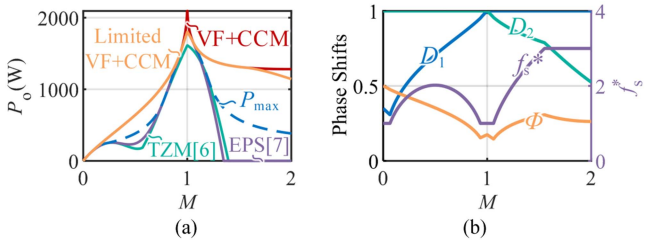

Fig. 11. Key features of different controls. (a) Power comparison under $I_{\mathrm{Lim}} = 0.35I_N$ and f_s^* is limited to [1] and [3]. (b) Control variable variation under frequency limitation.

Fig. 12. Hardware prototype.

can be seen, the CCM mode exhibits the highest PPS capability among all the controls. However, its application range is limited. The CCM control can only be used when $2M(1-M) \le I_{\mathrm{lim}} \le 1$, i.e., 0.42 in Fig. 5.

To extend the application range, Fig. 6 shows the current stress variation of CCM control at different unified switching frequency f_s^*.

As illustrated, the minimum value of $I_{\max}^*$ decreases with increasing f_s^*. For example, increasing f_s^* from 1 to 2 would extend $I_{\max}^*$ from 0.42 to 0.2. Moreover, at the same current

TABLE I
EXPRESSIONS OF PROPOSED VF+CCM CONTROL SCHEME

Modes	Optimal expressions of {D_1, D_2, Φ, and f_s}	Output power P_o
Buck mode	$D_1=1-\frac{(1-2\Phi)(M-1)}{M}, D_2=1, \Phi=0.5\left(1-\frac{M(1-4f_sLI_{Lim}/V_1)}{(M-1)^2+M^2}\right), f_{s,opt}=\frac{V_1\sqrt{2M(1-M)}}{4LI_{Lim}}$	$\left(1-\frac{(1-4f_sLI_{Lim}/V_1)^2}{(M-1)^2+M^2}\right)\cdot\frac{V_1V_2}{8f_sL}$
Boost mode	$D_1=1, D_2=1-(1-2\Phi)(M-1), \Phi=0.5\left(1-\frac{M-4f_sLI_{Lim}/V_1}{(M-1)^2+1}\right), f_{s,opt}=\frac{V_1\sqrt{2(M-1)}}{4LI_{Lim}}$	$\left(1-\frac{(M-4f_sLI_{Lim})^2}{(M-1)^2+1}\right)\cdot\frac{V_1V_2}{8f_sL}$

stress level ($I^*_{\max}=0.42$), there exists an optimal frequency ($f^*_s=1.5$) that enlarges p from 0.42 to 0.52.

The influence of f^*_s on output power can be explained by Fig. 7. In the VF+CCM control, as f^*_s increases from 1.0 to 1.65, the active power (purple area) remains essentially unchanged, while the backflow power (gray area) increases with the rise of Φ. According to the following equation:

$$P_o=\frac{1}{T_s}\int_0^{D_2T_{hs}} v_2 i_L dt$$

although the integral term $v_2 \cdot i_L$ decreases, the period T_s decreases with increasing f_s, leading to a possible increase of P_o. However, when $f^*_s=2.2$, the backflow power significantly increases, resulting in a reduced P_o. In addition, since algorithms in [6] and [7] transition to SPS control under boost conditions, their output power is significantly lower than that of CCM control under the same current stress.

Therefore, it is feasible to adjust f_s to extend the application range of CCM control and further increase output power at the same I_{Lim} level. Combined with (1) and (2), the optimal control law of VF+CCM control under both the buck and boost conditions can be readily obtained, as summarized in Table I.

IV. PROPOSED VF+CCM CONTROL

A. Control Loop Design

Based on the aforementioned analysis, a novel VF+CCM control is proposed, with its control loop illustrated in Fig. 8. The specific control process is listed as follows.

1) *Stage I:* Upon receiving the start-up command, the proportional–integral output I_{Lim} surges to the safe current limit I_{safe} defined by the saturation function. All the control variables are determined, as specified in Table I.
2) *Stage II:* When $V_2 \geq 0.95V_{2\text{ref}}$ is detected, the system prepares to transition to steady-state operation. The frequency is smoothly regulated and fixed at the steady value f_{steady}.
3) *Stage III:* When $V_2 \geq V_{2\text{ref}}$ is detected, the system enters steady operation. Under no-load conditions, I_{Lim} is automatically reduced to 0 to maintain a constant output voltage.

B. Maximum Output Power Characteristic

With the proposed VF+CCM control, the maximum PPS operation can be realized in a wide voltage gain, as shown in Fig. 9(a). Furthermore, the proposed control's output power even exceeds the theoretical maximum value of phase-shift control ($P_{\max}$) under fixed f_s, which is attributed to the introduction of frequency regulation.

Moreover, as shown in Fig. 9(b), benefiting from a single CCM phase-shift mode, all the phase-shift angles and frequencies can be smoothly adjusted without mode transition, which helps suppress dc bias caused by abrupt control variations.

C. Zero-Voltage Switching Characteristic

Since the proposed control primarily relies on increasing frequency to enhance the start-up speed, the switching losses might be exacerbated under high switching frequencies. Therefore, it is necessary to analyze the zero-voltage switching (ZVS) characteristics of the proposed control.

Based on the phase-shift definition in this letter and the symmetry of the inductor current, the per-unit turning-ON current expressions for each switch can be derived as follows:

$$\begin{cases} I(t_{S1})=D_1(M-1)-2M\Phi \\ I(t_{S4})=-D_1(M+1)+2M\Phi+2M \\ I(t_{Q1})=D_2(M+1)+2\Phi-2 \\ I(t_{Q4})=D_2(M-1)+2\Phi. \end{cases} \tag{3}$$

Combining the phase-shift angles and frequency expressions in Table I, each current expression can be simplified as follows (taking boost condition as an example):

$$\begin{cases} I(t_{S1})=I(t_{S4})=\frac{2(M-1)-M\sqrt{2(M-1)}}{(M-1)^2+1} \\ I(t_{Q4})=\sqrt{2(M-1)} \\ I(t_{Q1})=\sqrt{2(M-1)}-\frac{2(M-1)\left(M-\sqrt{2(M-1)}\right)}{(M-1)^2+1}. \end{cases} \tag{4}$$

As can be seen, each turning-ON current is only related to M. Therefore, current variation curves for each switch can be directly obtained, as shown in Fig. 10(a). Combining the per-unit value of the inductor current $I_N=V_1/(4f_sL)$, practical turning-ON currents can be obtained, as shown in Fig. 10(b). As seen, switching currents $I_{S1}=I_{S4}<0$ and $I_{Q4}>I_{Q1}>0$, indicating that ZVS operation of all the switches can be realized by VF+CCM control.

Due to the operation symmetry of DAB converters, similar conclusion can be obtained under the buck condition.

D. Determination Principle of Frequency Range

Fig. 11(a) and (b) further illustrates the output power and control variable changes under the unified frequency limitation [1], [3], respectively. As shown, setting the minimum switching frequency $f^*_{s\min}$ to 1, i.e., the steady-state operating frequency, only results in a slight power loss near $M=1$. Therefore, $f_{s\min}$ can be set as f_{steady} to avoid the issue of transformer saturation.

For the upper limit frequency $f_{s\max}$, since ZVS operation of all the switches can be realized during the start-up process, increasing the frequency does not lead to a significant rise in losses. Furthermore, as the start-up of the DAB converter is a

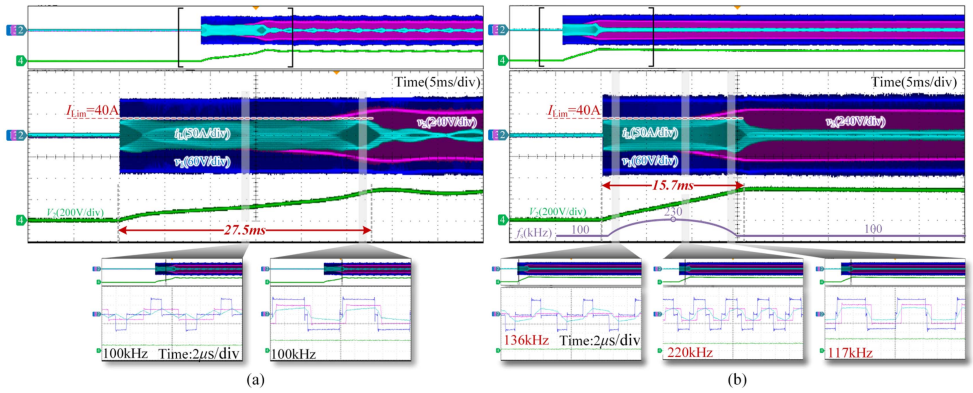

Fig. 13. Voltage-match condition start-up comparison under $V_1 = 100$ V, $V_{2\mathrm{ref}} = 250$ V, $M_{\mathrm{ref}} = 1$, $P_o = 0$ W, and $f_{\mathrm{steady}} = 100$ kHz. (a) EPS [7]. (b) Proposed.

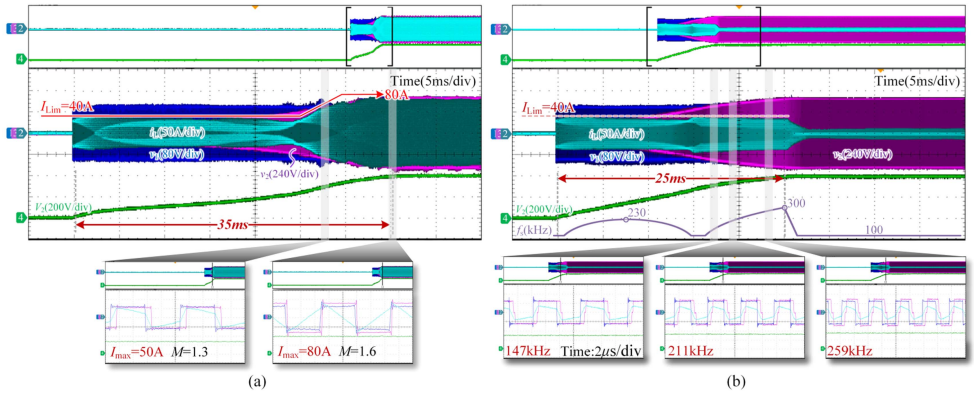

Fig. 14. Boost condition start-up comparison under $V_1 = 100$ V, $V_{2\mathrm{ref}} = 400$ V, $M_{\mathrm{ref}} = 1.6$, $P_o = 0$ W, and $f_{\mathrm{steady}} = 100$ kHz. (a) EPS [7]. (b) Proposed.

TABLE II
SYSTEM SPECIFICATIONS

Items	Value
Rated power P_o	2 kW
Input voltage V_1	100 V
Output voltage V_2	250–400 V
Frequency range f_s	100–300 kHz
Transformer T	n = 1:2.5
Inductors L_1 L_2	2 and 13 μH
Output capacitor C_2	470 μF

TABLE III
START-UP TIME COMPARISON AMONG STATE-OF-THE-ART CONTROLS

Condition	TZM [6]	EPS [7]	VF+CCM
M_{ref}=0.4	13.7 ms	9.8 ms	5.7 ms (58.4%, 41.8%)
M_{ref}=0.6	23.1 ms	16.6 ms	9.5 ms (53.1%, 42.2%)
M_{ref}=0.8	31.3 ms	22.6 ms	12.4 ms (60.4%, 45.1%)
M_{ref}=1.0	43 ms	27.5 ms	15.7 ms (63.5%, 43%)

millisecond-level transient process, the short-term accumulation of losses is unlikely to cause a significant temperature rise in the power devices. Therefore, $f_{s\max}$ can be directly derived from Table I. Taking the hardware parameters of Table II into Table I, $f_{s\max}$ in this letter is calculated to 300 kHz.

V. EXPERIMENTS

The DAB converter used for the experiment is illustrated in Fig. 12, with detailed parameters provided in Table II.

Notably, I_{Lim} on the V_1 side is set to 40 A. To prevent device damage, relatively high drain–source currents are selected for switches S_x ($I_D = 100$ A@$T_J = 25$ °C) and Q_x ($I_D = 35$ A@$T_J = 25$ °C). The steady operational frequency $f_{\mathrm{steady}} = 100$ kHz.

A. Verification of the Start-Up Process

A. 1) Voltage-Match Condition: The start-up processes of EPS [7] and VF+CCM controls are shown in Fig. 13. As can be seen, I_{Lim} can be actively controlled to 40 A by both the controls. However, through frequency regulation, the start-up time of VF+CCM control is reduced from 27.5 to 15.7 ms, achieving a 43% reduction. Furthermore, the start-up times of TZM control, EPS control, and proposed control under $M_{\mathrm{ref}} = [0.4, 1.0]$ are tested and listed in Table III, demonstrating that the proposed control features the fastest start-up speed.

A. 2) Boost Condition: The start-up processes of EPS and VF+CCM controls under $M_{\mathrm{ref}} = 1.6$ are shown in Fig. 14. Similarly, combined with VF+CCM control, the start-up time can be reduced from 35 to 25 ms. More importantly, for EPS control, which transitions to SPS control under the boost condition, the

TABLE IV
COMPARISON AMONG STATE-OF-THE-ART START-UP CONTROLS

Reference	Control features			Start-up features	
	Buck	Boost	Mode transition	Suitable operational range	Speed under M_{ref}=1
Ref [4]	Open + closed-loop		Five types	Buck condition	97 ms
TZM [6]	TPS+EPS	SPS	Three types	Buck condition	43 ms
EPS [7]	EPS1+EPS2	SPS	Three types	Buck condition	27.5 ms
VF+CCM	CCM	CCM	No need	Buck + boost condition	15.7 ms

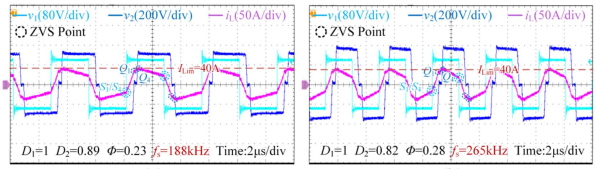

(a) (b)

Fig. 15. Steady waveforms of the proposed control. (a) $M = 1.2$, $V_2 = 300$ V, $f_s = 188$ kHz. (b) $M = 1.4$, $V_2 = 350$ V, and $f_s = 265$ kHz.

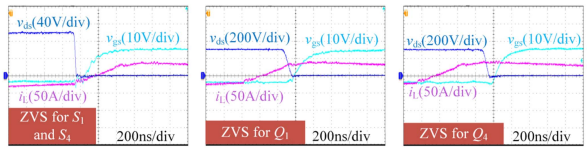

(a) (b) (c)

Fig. 16. Key ZVS waveforms of VF+CCM control under $V_1 = 100$ V, $V_2 = 300$ V, $f_s = 188$ kHz, $I_{\rm Lim} = 40$ A. (a) S_1 and S_4. (b) Q_1. (c) Q_4.

current stress cannot be maintained at 40 A when $M > 1.2$. To achieve start-up in a wide voltage range, $I_{\rm Lim}$ of EPS control must be relaxed, resulting in an exaggerated current stress of 80 A at $M = 1.6$. However, for VF+CCM control, $I_{\rm Lim}$ can be maintained at 40 A across the entire voltage range, effectively extending the safe start-up capability of the converter.

Notably, the dc bias phenomenon is hard to be observed in both Figs. 13(b) and 14(b), since the adjustments of frequency and phase shifts in each adjacent period are relatively small under the millisecond-level process. Furthermore, in each subfigure, whose total display duration is 20 μs, switching frequency remains constant as the control period is set to 100 μs.

B. Verification of ZVS Operation

To verify the ZVS characteristics of the proposed control, Fig. 15 presents the steady-state waveforms under VF+CCM control at different voltage points, where the ZVS point indicates that corresponding switch achieves ZVS operation. As observed, S_1 and S_4 turn ON with negative current. Q_1 and Q_4 turn ON under positive current, meaning that ZVS operation is realized.

Fig. 16 further illustrates the detailed ZVS states of all the switches in Fig. 15(a), where the ZVS states of S_1 and S_4 can both be represented by Fig. 16(a) since both the switches turn ON simultaneously. As observed, the drain–source voltages $v_{\rm ds}$ of all the switches fall to zero before the rise of the gate signal $v_{\rm gs}$, and inductor current flows through the antidiode of the switches, indicating that ZVS operation of all the switches is achieved by the VF+CCM control.

Finally, a detail comparison among [4], TZM [6], EPS [7], and proposed control is listed in Table IV. In summary, the proposed VF+CCM control operates solely in a single CCM mode, eliminating the need for mode transitions and, thus, resulting in a highly simplified control scheme. Furthermore, by incorporating frequency regulation, the proposed control method offers the broadest safe start-up range and the fastest start-up speed.

VI. CONCLUSION

This letter proposes an ultrafast and wide-safe-range start-up control scheme for DAB converters. First, an EPS-based CCM control featuring the maximum PPS capability is analyzed and introduced. By integrating frequency regulation, the maximized PPS capability of CCM control can be maintained under any current stress limitation, thereby enhancing the speed and safe range of the start-up process. Consequently, a VF+CCM control is established, enabling the entire start-up process to be accomplished within a single CCM mode, thereby eliminating complex mode transitions and simplifying the control system. Experimental results indicate that the proposed control achieves a broader safe start-up range, 43% faster start-up speed under voltage-match condition, and ZVS operation for all the switches.

REFERENCES

[1] J. Chen, C. Wang, and J. Chen, "Investigation on the selection of electric power system architecture for future more electric aircraft," *IEEE Trans. Transp. Electrific.*, vol. 4, no. 2, pp. 563–576, Jun. 2018.
[2] S. Pugliese, G. Buticchi, R. A. Mastromauro, M. Andresen, M. Liserre, and S. Stasi, "Soft-start procedure for a three-stage smart transformer based on dual-active bridge and cascaded H-bridge converters," *IEEE Trans. Power Electron.*, vol. 35, no. 10, pp. 11039–11052, Oct. 2020.
[3] P. Yao, X. Jiang, and F. Wang, "Soft starting strategy of cascaded dual active bridge converter for high power isolated DC-DC conversion," in *Proc. IEEE Appl. Power Electron. Conf. Expo.*, 2020, pp. 1031–1037.
[4] J. Liu, J. Yang, J. Zhang, Z. Nan, and Q. Zheng, "Voltage balance control based on dual active bridge DC/DC converters in a power electronic traction transformer," *IEEE Trans. Power Electron.*, vol. 33, no. 2, pp. 1696–1714, Feb. 2018.
[5] G. G. Oggier, M. Ordonez, J. M. Galvez, and F. Luchino, "Fast transient boundary control and steady-state operation of the dual active bridge converter using the natural switching surface," *IEEE Trans. Power Electron.*, vol. 29, no. 2, pp. 946–957, Feb. 2014.
[6] J. Hu, S. Cui, and R. W. D. Doncker, "Closed-loop black start-up of dual active-bridge converter with boosted dynamics and soft-switching operation," *IEEE Trans. Power Electron.*, vol. 36, no. 10, pp. 11009–11013, Oct. 2021.
[7] X. Liu et al., "A simple and fast start-up strategy for dual-active-bridge converters with DC bias suppression," *IEEE Trans. Power Electron.*, vol. 38, no. 9, pp. 10629–10639, Sep. 2023.
[8] O. M. Hebala, A. A. Aboushady, K. H. Ahmed, and I. Abdelsalam, "Generic closed-loop controller for power regulation in dual active bridge DC–DC converter with current stress minimization," *IEEE Trans. Ind. Electron.*, vol. 66, no. 6, pp. 4468–4478, Jun. 2019.